Mon. Not. R. Astron. Soc. **267,** 577–588 (1994)

The discovery of a brake on the white dwarf in AE Aquarii

O. C. de Jager,[1] P. J. Meintjes,[1]★ D. O'Donoghue[2] and E. L. Robinson[3]

[1]*Space Research Unit, Department of Physics, PU for CHE, Potchefstroom 2520, South Africa*
[2]*Department of Astronomy, University of Cape Town, Rondebosch 7700, South Africa*
[3]*McDonald Observatory and Department of Astronomy, The University of Texas at Austin, Austin, TX 78712, USA*

Accepted 1993 October 29; Received 1993 August 27

ABSTRACT

We report the discovery of a rapid spindown of the 33-s rotation period of the white dwarf in AE Aqr at a steady rate of 5.64×10^{-14} s s^{-1} over a baseline of at least 14.5 yr. The newly derived orbital period by Welsh, Horne & Gomer is confirmed, and it is shown that the secondary star's absorption-line radial velocities provide the correct phasing for the 33-s oscillations if they originate at the white dwarf. The amplitude of the pulse-timing delays, $a_{\rm wd} \sin i = 2.04$ s, yields a white dwarf mass of between 0.9 and 1.0 $M_\odot$. The spindown power of the white dwarf is $-I\Omega\dot{\Omega} = 6 \times 10^{33}\, I_{50}$ erg s^{-1}, which exceeds the accretion luminosity of AE Aqr by a factor of ~ 120. A significant fraction of $-I\Omega\dot{\Omega}$ may be converted to the acceleration of particles as in a pulsar, which may explain the observed radio synchrotron emission and the reported γ-ray emission. We also give evidence that the secondary lies above the main sequence since the secondary mass inferred from the main-sequence mass–radius relationship is too large.

Key words: binaries: close – stars: individual: AE Aqr – novae, cataclysmic variables – stars: oscillations – stars: rotation – white dwarfs.

1 INTRODUCTION

AE Aquarii is a nova-like variable ($V \approx 10.0$–12.5) at a distance of ~ 80–160 pc (Bailey 1981; Warner, in preparation). The UV luminosity is $\approx 1.7 \times 10^{31}\ d_{100}^2\ (f_\nu/1\ \text{mJy})\ (2000\ \text{Å}/\lambda)$ erg s^{-1} (Horne, private communication), resulting in an accretion rate of $\approx 5 \times 10^{31}\ d_{100}^2$ erg s^{-1} when averaged over the flares. The detection of a stable 33.0767-s period (with a stronger first harmonic at 16.5384 s) led to its classification as a DQ Her-type magnetic cataclysmic variable (Patterson 1979). Soft X-rays pulsed at the 33-s period were seen with the *Einstein* IPC (Patterson et al. 1980). Radio and millimetre synchrotron emission (Bookbinder & Lamb 1987; Bastian, Dulk & Chanmugam 1988; Abada-Simon et al. 1993), as well as TeV γ-rays (quasi-periodic and burst-like), was reported by two independent groups (Bowden et al. 1992; Meintjes et al. 1992).

The discovery of the coherent oscillations by Patterson (1979) (hereafter P79) led to an explanation using a simple magnetic oblique rotator model. The accumulation of observational data on the optical pulse timings, however, as well as on the emission- and absorption-line radial velocity curves, has raised problems for the model and deepened the mystery about the origin of the oscillations (Robinson, Shafter & Balachandran 1991, hereafter RSB). A historical perspective of this is given in the next section. With the recent absorption-line radial velocity analysis by Welsh, Horne & Gomer (1993, hereafter WHG), this mystery has been solved, and a clear prediction for the location of the pulse timings has been given. The problems for the simple oblique rotator model of P79 are now resolved and we have learned that the emission-line orbit does not give a reliable trace for the orbit of the white dwarf, contrary to the conclusion of RSB.

Recently we have been acquiring optical photometry for use with TeV γ-ray studies (Meintjes et al. 1992), but, with the lack of an accurate ephemeris for the optical oscillations, the search for coherency time-scales of a few years in γ-rays has been difficult given the poor signal-to-noise ratio in γ-rays. De Jager (1991) has also shown that the pulsed X-ray signal is incoherent over a time-scale of 2 yr, given the supposedly stable optical period of RSB. Clearly, in view of the above, an investigation of the long-term behaviour of the optical oscillation is timely, and in this paper we report the discovery of a rapid spindown of the 33-s oscillations, by analysing the 16.5-s arrival times (since the 33-s pulse profile is a double sinusoid, but the two peaks have different amplitudes). We use data over a baseline of 14.5 yr (i.e. between 1978 and 1992). All arrival times have been converted to Barycentric Ephemeris Time, which is also the time standard for radio pulsar timing. We also derive the orbital elements,

★Present address: Max-Planck-Institut für extraterrrestrische Physik, 85740 Garching bei München, Germany.

and show that the orbital period and phase zero are consistent with the absorption-line ephemeris of WHG.

2 AN HISTORICAL OVERVIEW

2.1 The emission-line, absorption-line and pulse-timing orbits

With the discovery of the 33-s oscillations, P79 proposed an oblique rotator model and showed that these oscillations (using the 16.5-s pulse timings) are consistent with a Doppler curve that is 180° out of phase with that of the red secondary star when using the absorption-line ephemeris of Payne-Gaposchkin (1969). The associated radius of the pulse-timing orbit was found to be 2.40 ± 0.09 s.

RSB found that the phasing of the emission-line orbit is consistent with the phasing of the absorption-line orbit obtained from Feldt & Chincarini (1980). RSB also showed that the emission-line orbit passes two primary tests for reliability as a tracer of the orbit of the white dwarf: it is circular, and it is 180° out of phase with the absorption-line orbit to within measurement errors. Furthermore, the amplitude of the radial velocity variation appears to be insensitive to measurement technique. Surprisingly, the pulse-timing orbit appeared to be distorted (with a mean semi-amplitude of 2.30 ± 0.07 s), and phase-shifted by 60° relative to the emission-line orbit. As a result, RSB proposed the idea of reprocessing of EUV or X-rays from the white dwarf to give the optical pulsations with a distorted optical pulse-timing orbit at a position near the edge of the Roche surface. In this case the X-ray pulse frequency should differ from the optical pulse frequency by the orbital frequency, and the X-ray pulse-timing orbit should coincide with the emission-line orbit.

De Jager (1991) specifically addressed the above-mentioned issues when reanalysing the *Einstein* IPC data on AE Aqr, and found that (i) the X-ray period is equal to the optical period (see also Eracleous, Patterson & Halpern 1991), and (ii) the X-ray pulse-timing orbit follows the optical pulse-timing orbit, and not the emission-line orbit. Considering these findings along with the result of RSB, de Jager (1991) was forced to conclude that the X-rays must also be the result of reprocessing, raising the question: where is the direct pulse from the white dwarf? In an attempt to provide an answer, Marsh (1992) then developed a model in which it was shown that the pulsations occur on the spin rather than the beat period even with reprocessing from azimuths corresponding to the bright-spot/gas stream region to explain the 60° orbital phase delay.

Clarification of these problems began with the high-speed, high spectral resolution spectrophotometry obtained by Welsh, Horne & Oke (1993): it was shown that the optical oscillation spectrum is quite blue $f_\nu \propto \nu^{0.9}$, and a small blackbody ($T > 12\,400$ K with an emitting radius of less than 10^9 cm^2) could produce the observed spectrum. This small area would argue against any reprocessing model and place the origin of the pulsations on, or near, the white dwarf. In the most important further development, WHG presented the results from simultaneous emission- and absorption-line radial velocity measurements, and found that the absorption-line ephemeris of Feldt & Chincarini (1980) lacked accuracy. WHG derived a more accurate absorption-line ephemeris: the time of superior conjunction of the white dwarf, i.e. when the red star is between us and the white dwarf, is

$$T_0 = \text{HJD } 243\,9030.7898(11) + 0.411\,655\,601(56)E. \quad (1)$$

As a result of being forced to use the absorption-line ephemeris of Feldt & Chincarini, RSB, who had emission-line data only, found the two radial velocity curves to be antiphased. The improvement in accuracy by WHG has now led to a different conclusion: the emission- and absorption-line radial velocities are not antiphased by 180° (as claimed by RSB), but are in fact phase-shifted by ~180°–75°. Thus the emission-line orbit is not a reliable tracer of the white dwarf's orbital motion, the Hα emission line must be strongly contaminated by emission from material whose orbital motion differs from that of the white dwarf, and only the absorption-line radial velocity curve follows the binary orbit.

Whereas RSB found that the optical pulse-timing orbit is shifted by 60° relative to the absorption-line orbit, WHG's new ephemeris (equation 1) and optical pulse-timing data instead showed that the pulse-timing orbit is antiphased with the absorption-line orbit to within ($5\overset{\circ}{.}4 \pm 2\overset{\circ}{.}6$). Furthermore, RSB found that the pulse-timing orbit of P79 differs by ~180°–60° from the absorption-line ephemeris. This problem can now also be resolved: the time of superior conjunction of the optical pulse-timing orbit is around HJD 244 3715.8415 (from table 2 and fig. 10 of P79), giving a phase offset of $\sim 2\overset{\circ}{.}5$ with respect to equation (1). Thus there is again no significant phase offset relative to the absorption-line ephemeris when applying the correct orbital period as given by equation (1). Using the optical pulse timings, we will also show that the orbital period of equation (1) is preferred to the incorrect period of Feldt & Chincarini.

2.2 The oscillation period and its stability

P79 obtained a coherent 16.5-s period of $P_{\rm P79} = 0.000\,191\,416\,306(20)$ d (heliocentric period) from data taken during 1978, and the constraint on the period change was found to be $-10^{-11} \leq \dot{P} \leq 7 \times 10^{-11}$. In a short note by Patterson, Beuermann & Africano (1988), a period derivative of $\dot{P} \leq 10^{-14}$ s s^{-1} was quoted, although no detailed information was given on how this was obtained. RSB have stressed the importance of using barycentric corrections instead of heliocentric corrections given such a short period, and obtained a barycentric period of $P_{\rm RSB} = 0.000\,191\,416\,425(1)$ from data taken between 1982 and 1983. They claimed that the difference between $P_{\rm P79}$ and $P_{\rm RSB}$ is due to the difference between barycentric and heliocentric corrections.

De Jager (1991) has reanalysed the three IPC X-ray observations (on a common time-base extending over a baseline of 2 yr) and found that the data set is inconsistent with the precise period of $P_{33} = 2P_{\rm RSB}$. The uncertainty in $P_{\rm RSB}$ would have resulted in a phase shift of only 0.02 when extrapolating back to the beginning of the *Einstein* observations. One possible explanation for this discrepancy is the presence of a period derivative which becomes detectable over a baseline of at least 2 yr (note that the pulse period was determined by RSB using data covering only 1.1 yr). We discovered small errors in the barycentric corrections of RSB, however, which may change the period measurements also. We therefore have had to reanalyse all the available

optical pulse timings using a single time standard, as presented below.

3 NEW OBSERVATIONAL DATA

In order to fill up the time gaps in already published timings, and to maximize the length of the time-base, we obtained pulse timings from new or unpublished photometric observations which were made by ourselves and various other observers who have kindly provided their data. In Table 1 we list all such photometric observations. The observations with an 'M' prefix to the run number have been made at the McDonald Observatory by various observers; see Nather (1973) and RSB for a description of the equipment used for the photometric observations. The one observation with a 'B' prefix to the run number has been made with the 1.6-m telescope of the Brazilian Astrophysical Observatory (see Jablonski 1981). The rest of the photometric observations (with an 'S' prefix) have been made at the Sutherland site of the SAAO with the 0.76-, 1- and 1.9-m telescopes. The blue-sensitive University of Cape Town Photometer, which is similar to the one described by Nather (1973), was used at the Sutherland site for almost all the data. For the observation by M. Cropper, the UCT polarimeter was used with a $CuSO_4$ filter to isolate the blue region of the spectrum. The observation of C. Koen was made with the *U* filter. In all cases the individual integrations were between 1 and 5 s per point, and the runs lasted up to 6.5 h per night.

For the purposes of this paper we only had to subtract the sky background from each integration, and no correction for airmass was made, since we only had to do a timing analysis on sections of data without investigating the source intensity.

4 THE 16.5-s PULSE TIMINGS FROM THE PHOTOMETRIC OBSERVATIONS

We followed the prescription of RSB by excluding the strong flares from all analyses, since the presence of quasi-periodic oscillations (QPO) near the spin period may contaminate the otherwise coherent signal. RSB used a cosine bell data window to taper the ends of the segments, which reduces ringing and spectral leakage. We used a different technique, which has the same effect: the data were first pre-whitened by filtering out the low frequencies. This was done by subtracting a 100-s moving average from each integration point. We found that the final result was insensitive to whether or not the filter was applied. This is because we concentrated on the quiescent (i.e. flat) parts of the light curve, and the use of a filter is more important in the presence of flares.

A pulse timing was then obtained by fitting a sinusoid to about 72 cycles of the 16.538-s period (it has to be an integer number of cycles), covering about 1200 s per section. After fitting a sinusoid with the 16.538-s period, the phase of the oscillation was calculated from the sine and cosine moments to obtain the arrival time of the 16.5-s period, corresponding to the start of each 1200-s data section. The internal standard deviation of each fit was nearly always less than 1 s, which is small compared with the 16.5-s test period. We have recalculated some of the pulse timings of P79 and found nearly identical results, which shows that the result is independent of the technique used for determining the arrival time.

Each 16.5-s pulse timing was then transformed to Barycentric Julian Ephemeris Day (BJED), by using the PEP740 program of the MIT, which was kindly provided by J. F. Chandler. This program accepts the 1950.0 coordinates of a source and performs the necessary reductions to provide a correction that is accurate down to the submillisecond level. Notice that these times are about 50 s later than the corresponding Heliocentric Julian Dates, mainly due to the difference between Ephemeris Time and Universal Time (ET − UT). The results are listed in Table 2 as Ref. No. 2, which includes, amongst others, the JD and the BJED of each pulse timing. All other available pulse timings (revised if necessary) are also collected in Table 2 and discussed in the following section.

5 PUBLISHED 16.5-s PULSE TIMINGS

The 34 published pulse timings of P79 (JD 244 3668–3747) and the one given by Imamura & Steiman-Cameron (1988) on JD 244 6966 were given in HJD. However, it is not correct to use HJD for a 16-s period analysis over a time-span of 14-yr, and we had to transform their pulse timings to the BJED standard: for each of these pulse timings we subtracted the Heliocentric correction term (HJD − JD) (where JD is the Julian date obtained from the UTC of the pulse) to give the JD at Earth. After this each pulse timing was transformed to Barycentric Julian Ephemeris Day (BJED) as discussed in the previous section.

In Table 2 we also list the UTC (in terms of JD) and the corresponding BJED of these pulse timings. The individual pulse timings of RSB (JD 244 5172–5589) were listed in BJED, but, because of the discovery of errors in the barycentric corrections, these had to be revised by amounts of up to ±3 s. Eracleous & Horne (private communication) provided us with two pulse timings during 1989 (JD 244 7314–7315) and one during 1992 November (JD 244 8954) obtained with the *Hubble Space Telescope*.

6 THE 16.5-s ANALYSIS

We now attempt to derive an ephemeris for the oscillations such that the observed timings O_i (for $i=1, \ldots, n$) are correctly predicted by the calculated timings from the model $C_i = T_{\max} + E_i P_0 + \frac{1}{2} E_i^2 \dot{P} P_0$ [see e.g. equation (2) of Downs (1981) for a more general expression for C], where $T_{\max}$ is the time of pulse maximum and E is the cycle number for a period that changes with time at a rate of $\dot{P}$. The observed minus calculated $(O-C)$ times (in the units of P_0) are then given by

$$(O-C)_i = P_0 \times \mathrm{frac}\left[\frac{1}{P_0}(O_i - T_{\max}) - \frac{1}{2}\frac{\dot{P}}{P_0^2}(O_i - T_{\max})^2\right] \quad i=1,\ldots,n, \qquad (2)$$

where the 'frac[ ]' refers to the fraction of the expression in square brackets. One way to obtain the values of $T_{\max}$, P_0 and $\dot{P}$ is via χ^2 fitting, given that the error on each arrival time has been correctly specified. We have found that the internal standard deviation sometimes underestimates the true error, which results in an unreliable χ^2 fitting – especially when assigning confidence intervals to parameters. Since we want to minimize the scatter around all the observed minus calcu-

Table 1. Log of optical observations of AE Aquarii.

Run Number	Starting time Date ; Time	BJED Start 2440000+	Telescope (m)	Integration Time (s)	Duration (s)	Observer
M2202	07/06/78 09:45:40	3666.910481	2.08	2	3186	Patterson
M2215	09/06/78 09:30:20	3668.899985	2.08	2	3692	Patterson
M2220	29/06/78 09:25:30	3688.897932	0.92	1	3410	Patterson
M2223	25/07/78 06:02:10	3714.757635	2.08	3	12510	Patterson
M2227	26/07/78 05:42:00	3715.743645	2.08	3	16137	Patterson
M2228	27/07/78 04:35:10	3716.697246	2.08	3	2847	Patterson
M2229	27/07/78 06:17:01	3716.767976	2.08	3	1200	Patterson
M2233	28/07/78 09:52:00	3717.917284	2.08	3	1854	Patterson
M2245	02/08/78 09:51:31	3722.916982	2.08	3	4215	Patterson
M2254	08/08/78 03:08:01	3728.636764	0.92	3	25314	Patterson
M2259	09/08/78 08:42:15	3729.868862	0.92	3	4326	Patterson
M2262	10/08/78 04:38:10	3730.699352	0.92	3	4779	Patterson
M2264	10/08/78 07:34:20	3730.821689	0.92	3	5637	Patterson
M2272	27/08/78 02:13:42	3747.598644	0.92	3	2904	Patterson
M2276	27/08/78 08:39:06	3747.866273	0.92	3	3351	Patterson
M2388	27/04/79 10:08:45	3990.922837	2.08	1	3480	Robinson
M2391	28/04/79 09:47:16	3991.908011	2.08	1	4050	Robinson
M2407	24/06/79 07:03:20	4048.798915	0.92	2	5640	Patterson
M2409	25/06/79 06:56:00	4049.793882	0.92	2	4120	Patterson
M2424	28/06/79 08:45:50	4052.870330	0.92	2	2020	Patterson
M2442	01/07/79 07:29:10	4055.817245	0.92	2	7760	Patterson
M2447	11/08/79 05:57:00	4096.754101	2.08	2	4500	Patterson
M2449	15/08/79 04:06:50	4100.677542	2.08	2	12280	Patterson
B4438	18/07/80 03:41:00	4438.659482	1.60	1	3600	Jablonski
S2811	04/10/80 18:11:20	4517.261275	1.02	4	10760	Warner
M2691	22/07/82 08:00:23	5172.839688	0.92	3	10056	Kepler
M2692	23/07/82 07:16:00	5173.808885	0.92	5	3855	Kepler
M2694	25/07/82 08:45:00	5175.870726	0.92	3	7092	Kepler
M2703	20/08/82 07:14:00	5201.807402	2.08	5	6950	Kepler
M2711	23/08/82 06:23:10	5204.772019	2.08	3	3822	Kepler
M2728	12/10/82 01:57:51	5254.584655	2.08	1	1900	Robinson
M2730	14/10/82 01:47:02	5256.576966	2.08	1	10324	Robinson
M2734	15/10/82 01:49:20	5257.578474	2.08	1	4000	Robinson
M2735	15/10/82 03:08:14	5257.633261	2.08	1	2890	Robinson
M2738	16/10/82 01:47:53	5258.577377	2.08	1	10110	Robinson
M2741	18/10/82 01:38:57	5260.570992	2.08	1	3690	Robinson
M-SH2	13/07/83 05:04:26	5528.717238	0.92	1	10989	Hine
M-SH3	13/07/83 08:11:40	5528.847266	0.92	1	6800	Hine
M-SH4	15/07/83 07:18:19	5530.810282	0.92	1	10675	Hine
M2824	09/09/83 03:30:48	5586.651615	0.76	1	7013	Balachandran
M2825	09/09/83 05:51:27	5586.749283	0.76	1	11398	Balachandran
M2826	10/09/83 02:54:00	5587.626006	0.76	1	8773	Balachandran
M2827	10/09/83 05:25:07	5587.730943	0.76	1	12081	Balachandran
M2828	11/09/83 02:57:13	5588.628184	0.76	1	10147	Balachandran
M2829	12/09/83 03:18:26	5589.642860	0.76	1	18442	Balachandran
S3573	14/06/85 00:20:01	6230.518161	1.90	4	11880	Cropper
S3883	05/07/86 22:09:50	6617.429034	1.02	2	16110	O'Donoghue
S4034	29/04/87 02:26:20	6914.601858	1.02	2	4674	O'Donoghue
S4037	30/04/87 02:47:00	6915.616305	1.02	2	3898	O'Donoghue
S4039	31/04/87 02:18:00	6916.596259	1.02	2	5288	O'Donoghue
S4043	04/05/87 01:35:20	6919.566909	1.02	2	2150	O'Donoghue
S4045	04/05/87 02:14:25	6919.594053	1.02	2	3374	O'Donoghue
S5128	13/06/90 01:22:30	8055.561537	1.02	2	9708	O'Donoghue
S5129	14/06/90 02:25:01	8056.605027	1.02	2	5622	O'Donoghue
S5130	18/06/90 02:39:30	8060.615295	1.02	2	5554	O'Donoghue
S5302	14/09/90 17:55:00	8149.251476	1.02	1	2778	Buckley
S5304	14/09/90 22:19:00	8149.434798	1.02	1	5930	Buckley
S8416	09/06/91 01:26:44	8416.564173	0.76	1	9420	Meintjes
S8417	09/06/91 21:51:35	8417.414828	0.76	1	23697	Meintjes
S8418	10/06/91 21:42:16	8418.408433	0.76	1	22730	Meintjes
S8419	11/06/91 21:28:30	8419.398947	0.76	1	23540	Meintjes
S8422	14/06/91 21:13:46	8422.388931	0.76	1	23180	Meintjes
S8830	26/07/92 19:44:41	8830.328933	0.76	1	10040	Meintjes
S8831	27/07/92 23:46:11	8831.496655	0.76	1	7650	Meintjes
S8855	20/08/92 18:58:23	8855.296601	0.76	1	7990	Koen

Table 2. Times of pulse maxima (JD and BJED), orbital phase, and phase residual of the 16.5-s timings.

JD of pulse 2440000+	BJED (frac.)	Ref. No.	Φ_{orb}	Resid. (cycles)	JD of pulse 2440000+	BJED (frac.)	Ref. No.	Φ_{orb}	Resid. (cycles)
3668.911524	.915446	1	0.01	-0.04	4048.794877	.799811	2	0.83	0.00
3688.892709	.897933	1	0.55	0.03	4048.819566	.824501	2	0.89	-0.05
3714.768017	.774148	1	0.41	-0.04	4049.793595	.798588	2	0.26	-0.11
3714.788498	.794629	1	0.46	-0.03	4052.866432	.871600	2	0.72	-0.02
3714.808979	.815110	1	0.51	-0.03	4055.835165	.840490	2	0.93	-0.03
3714.829459	.835591	1	0.56	-0.04	4055.856034	.861360	2	0.98	-0.01
3714.849940	.856072	1	0.61	-0.06	4096.757366	.763550	2	0.34	0.05
3714.870423	.876555	1	0.66	-0.08	4096.771154	.777338	2	0.38	0.10
3715.754028	.760174	1	0.80	0.03	4100.717845	.723974	2	0.96	-0.03
3715.774520	.780666	1	0.85	0.05	4100.745606	.751735	2	0.03	0.00
3715.815496	.821642	1	0.95	0.07	4438.653654	.659664	2	0.88	-0.08
3715.835964	.842111	1	0.00	0.00	4438.653647	.659657	2	0.88	-0.11
3715.856448	.862595	1	0.05	0.02	4438.674332	.680343	2	0.93	-0.07
3715.876925	.883072	1	0.10	0.01	4517.257926	.261331	2	0.82	0.01
3715.897412	.903560	1	0.15	0.08	4517.271908	.275312	2	0.86	0.02
3716.707660	.713819	1	0.12	0.03	4517.285708	.289111	2	0.89	0.09
3716.764863	.771022	1	0.26	-0.04	4517.299671	.303073	2	0.92	0.02
3717.927724	.933897	1	0.08	-0.04	4517.313458	.316859	2	0.96	0.03
3722.925182	.931389	1	0.22	0.02	4517.325131	.328531	2	0.99	0.00
3722.943362	.949569	1	0.27	0.03	5172.920199	.926289	3	0.57	0.02
3728.659446	.665643	1	0.15	-0.04	5173.819283	.825390	3	0.76	0.01
3728.733712	.739908	1	0.33	0.07	5175.865116	.871258	3	0.73	0.08
3728.750165	.756361	1	0.37	0.04	5175.886921	.893063	3	0.78	-0.04
3728.770637	.776833	1	0.42	0.02	5175.893632	.899774	3	0.80	0.00
3728.819826	.826022	1	0.54	0.00	5175.932122	.938265	3	0.89	0.03
3728.852761	.858957	1	0.62	0.03	5201.802134	.808147	3	0.73	-0.04
3728.873438	.879633	1	0.67	0.01	5201.834692	.840704	3	0.81	-0.01
3728.894120	.900315	1	0.72	0.02	5204.782030	.787961	3	0.97	0.02
3729.879164	.885352	1	0.12	-0.04	5204.800802	.806732	3	0.02	0.08
3729.899646	.905834	1	0.17	-0.01	5254.583641	.586455	3	0.94	0.05
3730.709734	.715915	1	0.13	0.01	5256.575669	.578307	3	0.78	0.01
3730.734417	.740597	1	0.19	-0.01	5256.595772	.598408	3	0.83	-0.01
3747.604694	.610491	1	0.18	-0.05	5256.614925	.617559	3	0.88	0.01
3747.604712	.610509	1	0.18	0.04	5256.634638	.637270	3	0.93	-0.04
3990.924604	.924698	2	0.24	-0.04	5256.654369	.656999	3	0.97	0.02
3990.938389	.938484	2	0.27	0.01	5256.673892	.676521	3	0.02	0.01
3990.952353	.952450	2	0.31	0.00	5257.630832	.633375	3	0.35	0.01
3991.909713	.909900	2	0.63	-0.04	5257.647676	.650217	3	0.39	0.02
3991.923506	.923694	2	0.66	0.01	5258.575749	.578207	3	0.64	0.02
3991.937474	.937663	2	0.70	-0.04	5258.595271	.597727	3	0.69	-0.03

Ref. 1: P79; Ref. 2: this work; Ref. 3: RSB.

5258.614619	.617073	3	0.74	0.00	5589.657585	.662643	3	0.92	0.04
5258.633576	.636029	3	0.78	0.00	5589.677672	.682728	3	0.96	-0.05
5258.653110	.655561	3	0.83	0.00	5589.759435	.764487	3	0.16	0.13
5258.672643	.675092	3	0.88	0.01	5589.795576	.800626	3	0.25	0.00
5260.569528	.571804	3	0.48	0.05	5589.814139	.819187	3	0.30	0.00
5260.590208	.592483	3	0.53	0.08	5589.832892	.837939	3	0.34	-0.01
5528.712116	.717942	3	0.87	-0.14	6230.516429	.520690	2	0.70	0.02
5528.728232	.734059	3	0.91	0.04	6230.530213	.534475	2	0.73	0.01
5528.747936	.753764	3	0.96	-0.03	6230.544189	.548452	2	0.77	0.01
5528.761331	.767159	3	0.99	-0.06	6230.557975	.562239	2	0.80	0.01
5528.775129	.780957	3	0.02	0.03	6230.571947	.576212	2	0.83	-0.02
5528.790246	.796075	3	0.06	0.01	6230.622876	.627145	2	0.96	0.01
5528.811105	.816935	3	0.11	0.01	6230.636664	.640934	2	0.99	0.04
5528.842110	.847941	3	0.18	0.04	6617.431710	.437249	2	0.60	-0.01
5528.862389	.868220	3	0.23	0.02	6617.444346	.449886	2	0.63	-0.01
5528.883814	.889646	3	0.29	-0.01	6617.472113	.477654	2	0.70	0.01
5528.902182	.908015	3	0.33	-0.01	6617.486092	.491634	2	0.73	0.02
5530.805412	.811307	3	0.95	0.01	6617.499869	.505411	2	0.77	-0.03
5530.831253	.837149	3	0.02	0.01	6617.513856	.519399	2	0.80	0.02
5530.855374	.861270	3	0.07	0.04	6617.527622	.533166	2	0.83	-0.08
5530.868194	.874091	3	0.11	0.03	6617.541617	.547161	2	0.87	0.01

Table 2 – *continued*

JD of pulse 2440000+	BJED (frac.)	Ref. No.	Φ_{orb}	Resid. (cycles)	JD of pulse 2440000+	BJED (frac.)	Ref. No.	Φ_{orb}	Resid. (cycles)
5586.695024	.700247	3	0.72	-0.03	6617.555397	.560942	2	0.90	-0.01
5586.711309	.716531	3	0.76	0.01	6617.569365	.574911	2	0.94	-0.05
5586.745182	.750402	3	0.84	-0.10	6617.583343	.588889	2	0.97	-0.03
5586.756691	.761911	3	0.87	0.01	6617.597132	.602679	2	0.00	0.01
5586.790391	.795609	3	0.95	0.02	6914.609762	.610000	2	0.50	-0.02
5586.811258	.816475	3	0.00	0.03	6914.621435	.621674	2	0.53	-0.03
5586.832134	.837350	3	0.05	0.09	6915.636857	.637192	2	0.99	0.01
5587.621937	.627110	3	0.97	-0.04	6915.650831	.651167	2	0.03	0.02
5587.643393	.648565	3	0.02	0.05	6916.635144	.635573	2	0.42	-0.01
5587.665393	.670563	3	0.08	-0.02	6916.649123	.649553	2	0.45	0.04
5587.684530	.689699	3	0.12	-0.03	6919.574454	.575160	2	0.56	0.03
5587.747306	.752472	3	0.28	0.02	6919.585946	.586653	2	0.59	0.06
5587.832096	.837257	3	0.48	0.06	6919.609665	.610375	2	0.65	-0.04
5588.624219	.629336	3	0.41	0.03	6919.623457	.624168	2	0.68	0.00
5588.643178	.648294	3	0.45	0.08	6966.771314	.775985	4	0.22	0.08
5588.678777	.683891	3	0.54	0.05	7314.870853	.874282	5	0.83	-0.14
5588.694856	.699969	3	0.58	0.04	7315.811016	.814522	5	0.11	-0.17
5588.711113	.716225	3	0.62	-0.06	8055.565367	.569613	2	0.13	0.03
5588.726449	.731560	3	0.65	0.04	8055.578166	.582413	2	0.17	-0.08
Ref. 4: Imamura & Steiman-Cameron (1988); Ref. 5: Eracleous & Horne (private communication).									
8055.592138	.596386	2	0.20	-0.06	8418.561843	.565936	2	0.93	-0.03
8055.605923	.610172	2	0.23	-0.01	8418.608166	.612263	2	0.04	-0.01
8055.621040	.625290	2	0.27	0.00	8418.621940	.626038	2	0.08	-0.04
8055.633662	.637913	2	0.30	-0.03	8419.402321	.406477	2	0.97	0.13
8055.647627	.651879	2	0.33	-0.05	8419.415698	.419855	2	0.00	0.01
8055.661591	.665844	2	0.37	-0.07	8419.429482	.433640	2	0.04	0.03
8056.608851	.613172	2	0.67	-0.05	8419.464310	.468470	2	0.12	0.02
8056.621503	.625825	2	0.70	0.03	8419.478077	.482238	2	0.16	-0.03
8056.651750	.656074	2	0.77	0.00	8419.536058	.540224	2	0.30	0.01
8060.618932	.623532	2	0.41	-0.03	8419.549832	.553999	2	0.33	-0.01
8060.631568	.636169	2	0.44	0.00	8419.563790	.567958	2	0.36	-0.06
8060.645541	.650143	2	0.48	0.01	8419.577753	.581922	2	0.40	-0.09
8060.659504	.664107	2	0.51	-0.04	8419.591540	.595710	2	0.43	-0.05
8060.670998	.675602	2	0.54	0.01	8419.605504	.609675	2	0.47	-0.08
8149.250722	.255670	2	0.72	0.03	8419.619279	.623451	2	0.50	-0.11
8149.263935	.268882	2	0.75	0.03	8422.392175	.396547	2	0.24	0.00
8149.433368	.438305	2	0.16	0.06	8422.405394	.409767	2	0.27	0.09
8149.493086	.498019	2	0.31	0.13	8422.419338	.423712	2	0.30	-0.04
8416.567824	.571767	2	0.09	0.01	8422.433140	.437515	2	0.34	0.10
8416.584661	.588605	2	0.13	0.00	8422.447088	.451464	2	0.37	-0.01
8416.608964	.612910	2	0.19	0.01	8422.461069	.465446	2	0.40	0.05
8416.636700	.640648	2	0.25	-0.03	8422.474839	.479217	2	0.44	0.01
8416.650488	.654437	2	0.29	0.03	8422.502597	.506977	2	0.50	0.04
8416.664446	.668396	2	0.32	-0.02	8422.516568	.520949	2	0.54	0.03
8417.439257	.443266	2	0.20	-0.02	8422.544311	.548694	2	0.61	-0.05
8417.453028	.457038	2	0.24	-0.05	8422.617259	.621647	2	0.78	-0.05
8417.466985	.470996	2	0.27	-0.10	8422.632206	.636595	2	0.82	0.02
8417.480957	.484969	2	0.30	-0.08	8830.336783	.343019	2	0.23	-0.03
8417.494761	.498774	2	0.34	0.07	8830.350575	.356812	2	0.26	0.05
8417.508717	.512731	2	0.37	0.00	8830.364541	.370778	2	0.29	0.04
8417.522506	.526521	2	0.41	0.06	8830.378305	.384542	2	0.33	-0.03
8417.536443	.540459	2	0.44	-0.11	8830.392284	.398521	2	0.36	0.02
8417.550254	.554271	2	0.47	0.05	8830.406055	.412292	2	0.39	-0.02
8417.564210	.568228	2	0.51	-0.03	8830.420028	.426265	2	0.43	-0.01
8417.578187	.582206	2	0.54	-0.01	8831.491614	.497864	2	0.03	0.02
8417.591982	.596002	2	0.57	0.05	8831.504423	.510673	2	0.06	-0.05
8418.411957	.416039	2	0.57	0.10	8831.518223	.524473	2	0.10	0.05
8418.425142	.429225	2	0.60	-0.02	8831.532199	.538449	2	0.13	0.08
8418.439134	.443218	2	0.63	0.06	8831.545971	.552221	2	0.16	0.05
8418.492343	.496431	2	0.76	-0.04	8831.559939	.566190	2	0.20	0.05
8418.506335	.510424	2	0.80	0.04	8855.291185	.297242	2	0.84	0.07
8418.520107	.524197	2	0.83	-0.03	8855.305358	.311415	2	0.88	0.10
8418.534096	.538187	2	0.86	0.04	8855.318755	.324811	2	0.91	0.06
8418.547870	.551962	2	0.90	-0.02	8954.355392	.353875	5	0.47	0.13

lated cycles (or phases) $\phi_i=(O-C)_i/P_0$, an obvious choice would be to maximize the inverse of the sample variance

$$s^{-2}=\left[\frac{1}{n-1}\sum_{i=1}^{n}(\phi_i-\bar{\phi})^2\right]^{-1}, \quad \text{with} \quad \bar{\phi}=\frac{1}{n}\sum_{i=1}^{n}\phi_i. \qquad (3)$$

Since we also find the time $T_{\max}$, corresponding to the time of pulse maximum, the term $\bar{\phi}=0$ at the optimal choice. This procedure would lead to a best estimate of the period parameters given the n pulse timings.

It is known (P79; RSB) that the observed pulse timings of Table 2 will include the binary orbital time delays of $\pm\sim 2$ s. We therefore first corrected the timings in Table 2 by the following approach: because the components (primary and secondary) of cataclysmic variables have circular orbits, we have fitted a circular orbit to the pulse timings with the time of superior conjunction of the pulse-timing orbit given by $T_0=$BJED 244 5172.2785. This time was obtained after adding an integer number of orbital periods to the zero time of HJD 243 9030.7879 given by WHG, as well as the offset between BJED and HJD, which is mainly due to the ~50-s offset between ET and UT. We also used the value of 2.3 s given by RSB for the semi-amplitude of the Doppler delays to remove the binary orbital delay.

P79 was able to determine the 16.5-s period unambiguously within one independent Fourier spacing (i.e. $\Delta P=P_0^2/\Delta T=5\times10^{-10}$ d) given by the time interval of the observations of $\Delta T=79$ d. The period determined by RSB from later data differed by only $\sim10^{-10}$ d from that of P79, which is significantly less than the ΔP of P79. RSB also found no significant period change inside their 417-d time-base. We have therefore grouped the data into subsets of similar length, both to maintain a reasonable period resolution of less than 10^{-10} d and in the expectation that the changes in period are undetectable in this time span. A total of six such subsets were constructed, and the time interval of each subset (covering between 1 and 1.9 yr per subset) is indicated in Fig. 1, which shows a plot of the inverse variance for each subset with $\dot{P}=0$. The period range of a few times 10^{-10} d shown in Fig. 1 covers a comfortable interval around the expected period, including all uncertainties in period, at least for the epoch between 1979 and 1983. The reference period corresponds to P_0 given below. The six periodograms are presented in Fig. 1 in the form of a projected 2D plot, with time increasing on the vertical scale.

The effect of aliasing (~1 cycle per yr or $\Delta P\sim10^{-10}$ d) due to the non-uniform spread of observations within each subset is obvious. To see if there is any trend in the period with time, the period corresponding to each significant peak of Fig. 1 has been carried over as a dot to the vertical scale of Fig. 2, and the mid-time of each subset has been used on the horizontal time-scale. The effect of aliasing is again visible for each subset as multiple dots at a given time, but we have introduced another dimension in Fig. 2, which is the significance of each peak: the size of each dot is proportional to the ratio $s^{-2}/s^{-1}_{\max}$, where s^{-2} is the amplitude of a particular peak, and $s^{-2}_{\max}$ is the amplitude of the largest peak of that same plot in Fig. 1. Thus the largest dot for each subset in Fig. 2 corresponds to the most significant period for that same time interval. The largest dots indicate a clear increase in the period, which is shown as a straight-line fit in Fig. 2. This increase in period is also shown as a dashed line in Fig. 1.

To obtain a solution for all subsets combined, we have analysed all the data on a single time-base of 14.5 yr and scanned in period and period derivative. The period range ($\pm3\times10^{-10}$ d) covers almost the entire range shown in Figs 1 and 2, and the period derivative range ($\pm12\times10^{-14}$ d d^{-1})

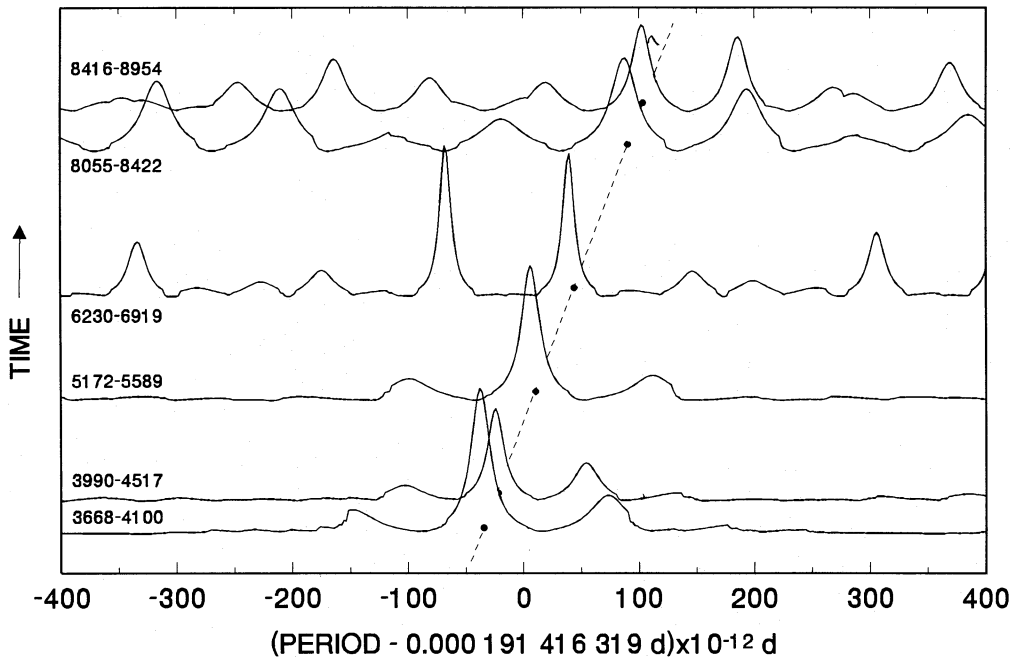

Figure 1. A projected 2D plot of six periodograms (inverse variance calculated as described in the text, projected on to the time domain) with time increasing up the vertical scale. The time interval corresponding to each plot (as JD 244 0000 +) is shown on the left side of each plot. The projected dashed line shows the period increase with time.

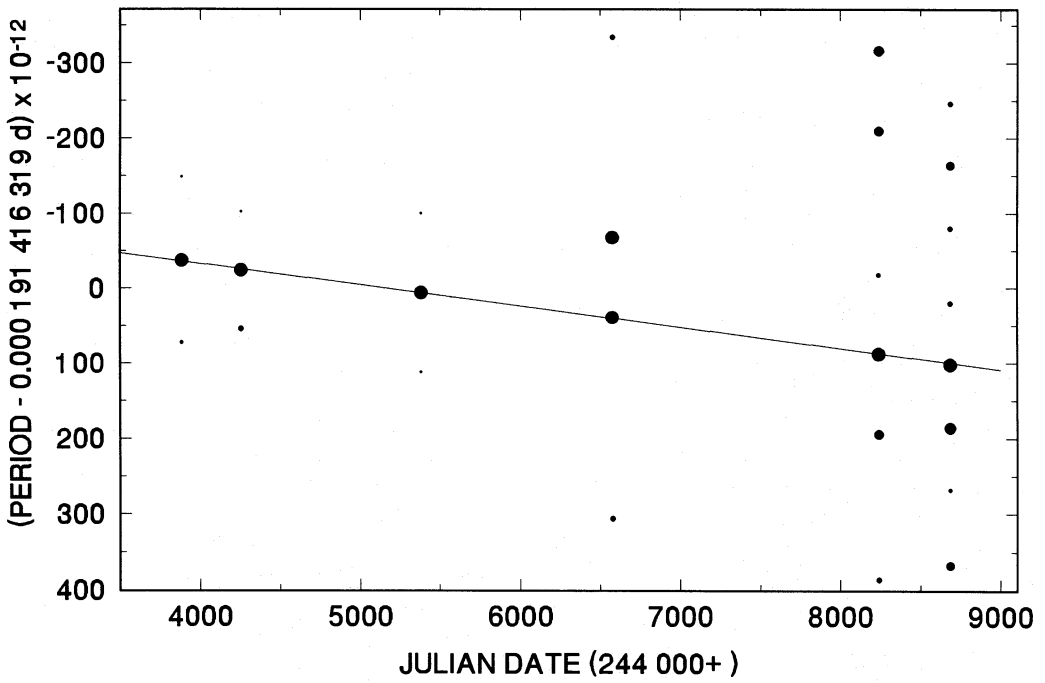

Figure 2. The period values (as dots) of the most significant peaks from each of the six periodograms shown in Fig. 1, as a function of the mean time (in terms of JD 244 000 +) corresponding to each time interval. The largest dot for each mean time corresponds to the most significant peak for that time, and the size of each dot is proportional to the significance (in terms of inverse variance) of its corresponding peak.

also covers a wide range of possibilities that can fit into Fig. 2. The results are shown as a surface plot in Fig. 3: a single significant peak protrudes above the noise level. This solution is the same as the straight-line fit in Fig. 2. The period at time BJED 244 5172.000 042 is $P_0 = 0.000\,191\,416\,3192$ d, and was used as the zero reference on the period scale of Figs 1–3. It is also at this period that the maximum in Fig. 3 is seen. The period derivative corresponding to the peak maximum is at $(2.82 \pm 0.01) \times 10^{-14}$ d d^{-1}, and this derivative is significant at the 280σ level. Thus the period and period derivative obtained from Figs 1–3 are unique, and, as discussed further below, the only solution that accounts for all the pulse timings in Table 2.

So far we have had to rely on the orbital parameters $P_{\rm orb}$ and T_0 given by WHG, and the amplitude of the Doppler delays given by RSB. To obtain the best solution we determined the best parameters in a 6D space: the time of the 16.5-s pulse maximum $T_{\rm max}$, the 16.5-s period corresponding to $T_{\rm max}$, the derivative of the 16.5-s period, the orbital period $P_{\rm orb}$, the time of superior conjunction of the pulse-timing orbit T_0, and the semi-amplitude of the Doppler orbit $a_{\rm wd} \sin i$ of the 16.5-s pulses. The inverse variance corresponding to the best solution is $s^{-2} = 423$, and the corresponding parameters are given in Table 3. Note that the period derivative given here corresponds to the 16.5-s period only. The errors in brackets refer to the last digit(s) of the number given, and were obtained from a formal least-squares fit.

Our orbital period differs from that of WHG by 1.1 × our quoted error, but differs from the orbital period of RSB (as obtained from emission-line radial velocities) by 4.4 × the total error (by 'total error' we mean the combination in quadrature of the errors given by RSB and ourselves). Thus the orbital period of WHG is clearly favoured by our data.[1] The time T_0 differs from that of WHG by 0.9 × the total error, but differs from the T_0 of RSB by only 0.3 × the formal error. Thus the values of T_0 from all three experiments are consistent with each other, and for future reference we use $P_{\rm orb}$ and T_0 given by WHG due to their better accuracy (but corrected for the difference in ET and UT as required for periodic sources outside the Solar system). Fixing these two parameters and repeating the optimization, we get the slightly (but not significantly) different period parameters given in Table 4. The maximum inverse variance is now 418. Note that we have multiplied the period and its derivative by two, so that a final set of elements can be given, which corresponds to the spin of the white dwarf. We have also analysed the 33-s pulse timings of P79, and the time $T_{\rm max}$ given here also predicts the 33-s maximum correctly. This also holds for the single pulse timing of Imamura & Steiman-Cameron (1988) and the pulse timings given by Eracleous & Horne (private communication), which are supposed to be equally as valid as the 33-s pulse timings.

The (O − C) curve for all the timings, relative to a constant period P_0 from Table 3, is shown in the top panel of Fig. 4 (after correcting for the Doppler delays): the neglect of the $\dot{P}$ term leads to the quadratic variation with time. The solid-line fit through the (O − C) values was obtained from the elements given in Table 4. The bottom panel shows the resid-

[1]Note that WHG's orbital period is inconsistent with RSB's orbital period and is determined much more precisely than our value.

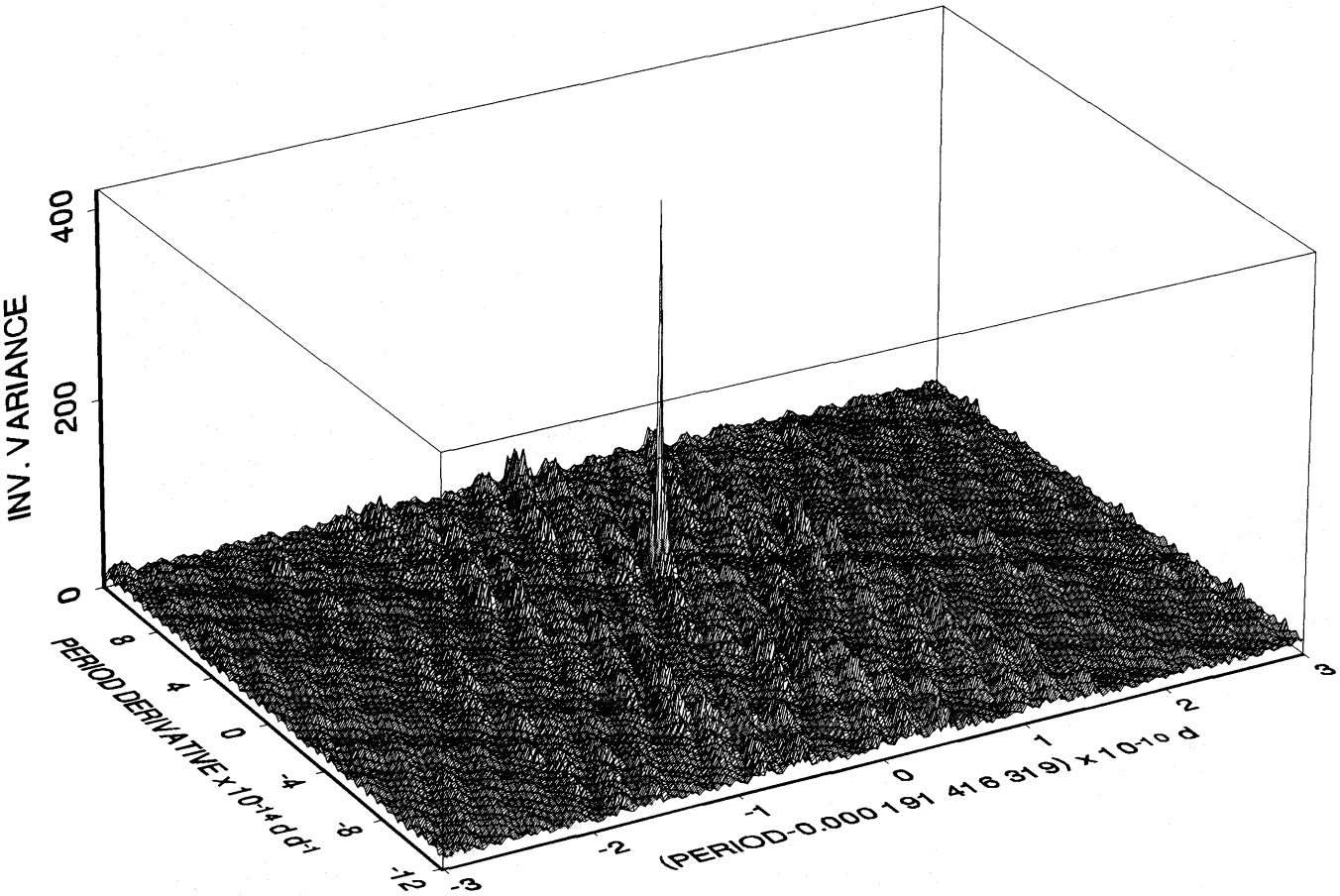

Figure 3. A plot of inverse variance versus $(P, \dot{P})$ for all the 16.5-s pulse timings of AE Aqr, shown here as a 3D surface plot. The inverse variance (calculated as described in the text) on the vertical scale is shown as a function of period (in units of 10^{-10} d) and period derivative (in units of 10^{-14} d d^{-1}) of the 16.5-s oscillation. The peak occurs at period 0.000 191 416 319 d and period derivative at 2.82×10^{-14} d d^{-1}.

uals after taking the $\dot{P}$ term into account. The distribution of residuals is shown in Fig. 5, and a normalized Gaussian distribution with a standard deviation of $\sigma = 1/\sqrt{418} = 0.05$ of the 16.5-s phase is shown for comparison. The fit appears to be satisfactory. The orbital phase $\phi_{\rm orb}$ and 16.5-s phase residual (obtained after applying the elements in Table 4) for each pulse timing are also given in Table 2.

In Fig. 6 we have plotted versus orbital phase the residuals of the timings with respect to the quadratic ephemeris, but omitting the Doppler corrections. This shows the behaviour of the orbital time delays alone. The average is around zero (due to the optimal choice of $T_{\rm max}$) as expected. The solid-line fit shows the cosine variation of the Doppler delay (with a 2.04-s semi-amplitude) due to the circular orbit that has been forced through the time delays. To see if these time delays really follow a circular orbit (RSB expressed doubts), these delays have been binned into 10 phase bins. The average and its corresponding standard error have been calculated for each bin. The results are shown as solid squares (with error bars) in Fig. 6. A χ^2 goodness of fit to the 10 points gives a value of $\chi^2_9 = 6.3$ for $10 - 1 = 9$ degrees of freedom (one less due to the freedom involved in $a_{\rm wd} \sin i$). Thus the pulse-timing orbit is circular within measurement error and no distortions are apparent. The error on $a_{\rm wd} \sin i$ obtained from the χ^2 technique[2] is 0.13 s. Our value of $a_{\rm wd} \sin i = 2.04 \pm 0.13$ s differs from the 2.30 ± 0.07 s of RSB by 1.9σ, and appears to be marginally inconsistent. We believe that our value and the circular orbit are closer to being correct, since we have a much larger data base. Furthermore, the heliocentric time standard (for P79), as well as the incorrect barycentric corrections of RSB, may have led to systematic errors in their determinations of $a_{\rm wd} \sin i$. We conclude that the ephemerides of Table 4 are a satisfactory representation of the times of maximum of the 16.5-s oscillations of AE Aqr thus far observed.

7 CONSTRAINTS ON THE MASSES OF THE PRIMARY AND SECONDARY IN AE AQUARII

The work of WHG shows that the absorption-line orbit gives the best available estimate of the orbital motion of the secondary, whereas the pulse-timing orbit (which is anti-phased with the absorption-line orbit as expected) gives a reliable estimate for the orbit of the white dwarf. This gives

[2]This error is reliable since the standard error on each of the 10 mean delays shown in Fig. 6 is Gaussian by virtue of the central limit theorem.

slightly different values (RSB & WHG) for the mass $M(2)$ of the secondary, the mass M_{wd} of the white dwarf primary, and the mass ratio q:

$$M(2)\sin^3 i = 0.33 \pm 0.03\ \mathrm{M}_\odot, \quad (4)$$

$$M_{wd}\sin^3 i = 0.48 \pm 0.03\ \mathrm{M}_\odot, \quad (5)$$

$$q = M(2)/M_{wd} = 0.684 \pm 0.044. \quad (6)$$

Combination of Kepler's equation

$$P_{orb} = \frac{4\pi^2 a^3}{G[M(2)+M_{wd}]}, \quad (7)$$

where a is the binary separation, with the equation for the volume radius R_V in a Roche-lobe-filling binary,

$$\frac{R_V}{a} = \frac{0.49\,q^{2/3}}{0.6\,q^{2/3}+\ln(1+q^{1/3})}, \quad (8)$$

leads to the equation for the mean density, which is independent of q within a few per cent and dependent only on the orbital period through the relation

$$\overline{\rho} = \frac{M(2)}{\frac{4}{3}\pi R_V^3} = 107\left(\frac{P_{orb}}{1\ \mathrm{h}}\right)^{-2}\ \mathrm{g\ cm^{-3}}. \quad (9)$$

For AE Aqr we find $\overline{\rho} = 1.1$ g cm^{-3}. From the $\overline{\rho}$–mass relationship for main-sequence secondaries (Webbink 1990; Warner, in preparation), it is found that the mass for secondaries can be written as

$$M(2) = (\overline{\rho})^{-0.635}\ \mathrm{M}_\odot \quad \text{for} \quad P_{orb} \leq 9\ \mathrm{h}. \quad (10)$$

This equation appears to hold for orbital periods down to at least 3.8 h. Applying this equation to AE Aqr (even though $P_{orb} = 9.88$ h), and assuming that the secondary of AE Aqr is a main-sequence star, for which equation (10) should hold, we arrive at a secondary mass of $M(2) = 0.94 \pm 0.15\ \mathrm{M}_\odot$ (the error reflects the typical scatter in the points given by Webbink). This mass is similar to that of a G5 dwarf star, but this solution can be excluded since the spectrum of AE Aqr's secondary is not that of a G5 star, but rather that of a later K-type star. An independent indication that the secondary is not a main-sequence star follows from the inferred primary mass of $M_{wd} = 1.37 \pm 0.24\ \mathrm{M}_\odot$ [when using equation (6) and assuming that equation (10) holds for AE Aqr], which is already at the maximum allowable mass of $\sim 1.36\ \mathrm{M}_\odot$ for a white dwarf. In fact, it was shown (Webbink

Table 3. The elements of the 16.5-s oscillations from pulse timings.

Time of 16.5 s maximum, T_{max}	BJED 2445172.0000423(10)
Period of 16.5 s oscillation, P_0	0.00019141631925(14) d
Derivative of 16.5 s period, $\dot{P}$	$2.821(10) \times 10^{-14}$ d d^{-1}
Time of superior conjunction, T_0	BJED 2445172.2828(50)
Orbital period, P_{orb},	0.4116548(7) d
Projected semi-amplitude, $a_{wd}\sin i$	2.04(13) s

Table 4. The elements of the white dwarf spin from pulse timings and absorption-line radial velocities.

Time of 33 s maximum, T_{max}	BJED 2445172.000042(1)
White dwarf period, P_{33}	0.00038283263840(28) d
Period derivative, $\dot{P}_{33}$	$5.642(20) \times 10^{-14}$ d d^{-1}
Time of superior conjunction, T_0	BJED 2445172.2784(13)
Orbital period, P_{orb},	0.411655610(56) d
Projected semi-amplitude, $a_{wd}\sin i$	2.04(13) s

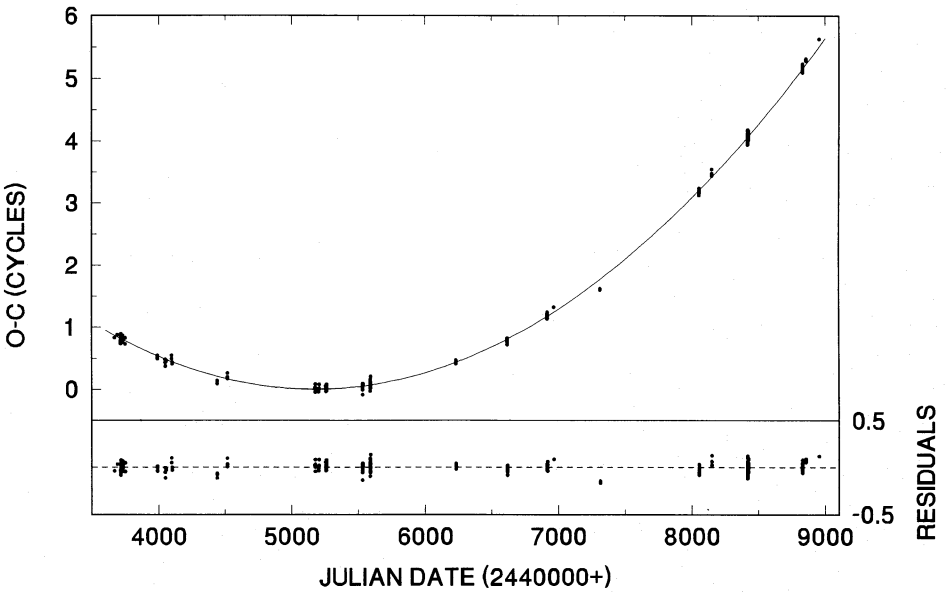

Figure 4. Top panel: the observed minus calculated phase (in cycles) of the 16.5-s pulse timings (after subtracting the Doppler delays using the parameters given in Table 4) as a function of time. The 'calculated' phase corresponds to a constant period of 0.000 191 416 3192 d and a reference epoch of T_{max} = BJED 244 5172.000 042. Bottom panel: the (O − C) residuals (also listed in Table 2) after taking the period derivative of 2.821×10^{-14} d d^{-1} into account.

1990; Warner, in preparation) that equation (10) holds only for $P_{orb} \leq 9$ h, and it is clear that the secondary in AE Aqr lies slightly above the main sequence.

Assumption of the mass range of $0.64 < M(2)/M_{\odot} < 0.70$ for the K-type secondary (RSB) results in a white dwarf mass (using equation 6) of $0.94 < M_{wd}/M_{\odot} < 1.02$.

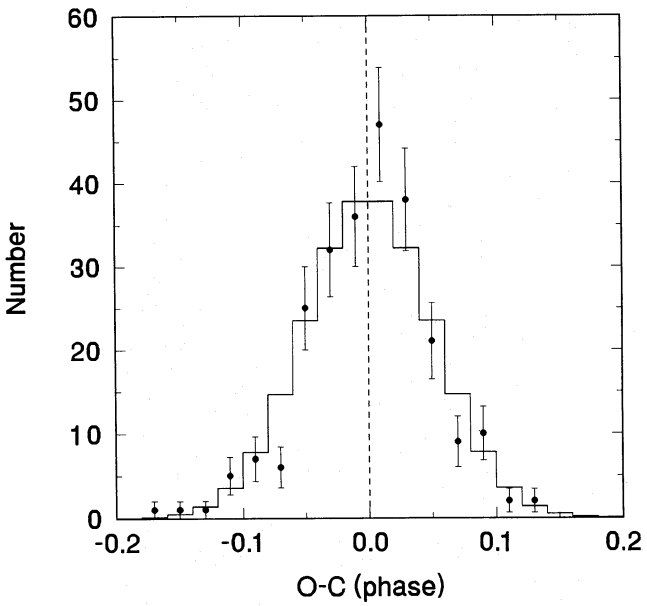

Figure 5. The distribution of phase residuals as listed in Table 2 and shown in the bottom panel of Fig. 4. Also shown is a normalized Gaussian distribution (and binned to the same scale) with a standard deviation of 0.05 cycles.

8 DISCUSSION

The most significant implication of our discovery that the white dwarf is spinning down is the spindown luminosity of $-I\Omega\dot{\Omega} = 6 \times 10^{33}\ I_{50}$ erg s^{-1}, which exceeds the accretion luminosity by a factor of $\sim 120\, I_{50} d_{100}^{-2}$, where I_{50} is the moment of inertia in units of 10^{50} g cm^2. Only the peak luminosity during the UV flares may become comparable with the spindown power.

It is clear that the loss of kinetic energy by the white dwarf is presently the main source of power in AE Aqr, and the white dwarf must have gained this kinetic energy in a recent time within the spindown time-scale of $P/\dot{P} \sim 2 \times 10^7$ yr. Interestingly, there is evidence that the accretion rate ($\dot{M}$) varies (or cycles) by orders of magnitude on time-scales of $T_c = 10$–10^5 yr (Warner 1987) in many cataclysmic variables (CVs). This time-scale is indeed much less than $P/\dot{P}$ and, according to the standard Ghosh & Lamb (1979) theory for accreting magnetized compact objects, a rotating compact object can be spun up if $\dot{M}$ is sufficiently large. We can therefore expect that a much higher $\dot{M}$ (say $\dot{M}^{max}$) than the present accretion rate of $\dot{M}^{present}$ would have resulted in a spin-up to a minimum period of $P_{min} = 33.08\ s - T_c\dot{P}$ within the expected cycle time $T_c < 10^5$ yr. Thus given the range expected for T_c, we expect $32.9\ s < P_{min} < 33.08$ s.

Furthermore, between the time T_c in the past and the present time, the accretion rate must have decreased from its maximum ($\dot{M}^{max}$) to the much smaller value ($\dot{M}^{present}$) at present, during which the white dwarf must have crossed from spin-up to spindown. The accretion rate at the time of equilibrium ($\dot{M}^{eq}$) would then obey the inequality $\dot{M}^{max} > \dot{M}^{eq} > \dot{M}^{present}$. The corresponding equilibrium period (that is when $\dot{P} = 0$) was then $32.9\ s \sim P_{min} < P_{eq} < 33.08$ s.

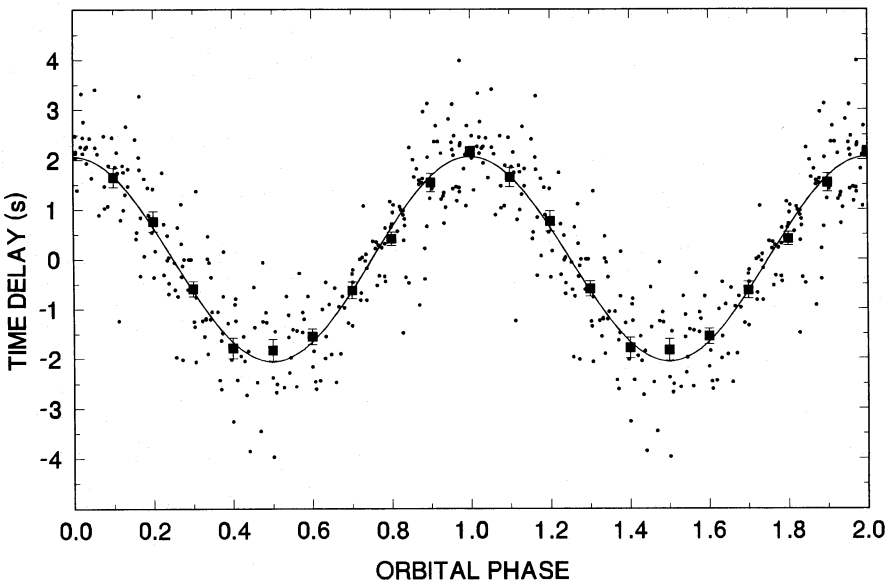

Figure 6. The pulse-timing orbit of AE Aqr. The figure shows the (O-C) diagram for the pulse timings of the 16.5-s period based on a test period of 0.000 191 416 3192 d at a reference time of BJED 244 5172.000 042 and a period derivative of 2.821×10^{-14} d d^{-1}. The (O − C) diagram has been folded on the orbital period of AE Aqr to give the pulse-timing orbit of the white dwarf. The solid line is the best-fitting circular orbit and yields a semi-amplitude of 2.04 ± 0.13 s. Each solid square indicates the mean of the time delays in 0.1 orbital phase interval bins. The error bars indicate the errors on the mean delays. The orbital phase has been repeated over two cycles.

Relation of $P_{eq} \sim 33$ s and $\dot{M}^{eq}$ via the equilibrium equation of Ghosh & Lamb (1979) gives an expression for the magnetic moment μ in the form

$$\frac{\mu_{32}}{\sqrt{\dot{M}_{18}^{eq}}} = 1.7\, M_1^{5/6} \left(\frac{\omega_c}{0.8}\right) \left(\frac{\phi}{0.5}\right)^{-7/4}, \qquad (11)$$

where $\dot{M}_{18}^{eq}$ is the equilibrium accretion rate in units of 10^{18} g s^{-1}, μ_{32} is the magnetic moment BR^3 in units of 10^{32} G cm^3, M_1 is the white dwarf mass in solar mass units, $\omega_c \sim 0.8$–0.9 is the critical fastness parameter (Ghosh & Lamb 1991) and $\phi \sim 0.5$ follows from angular momentum conservation.

Warner & Wickramasinghe (1991) also described the dependence of the spin period on the effect of magnetic cycling, and they have shown that the spin period will depend on $\dot{M}$ averaged over a long time-scale, which will, in turn, depend on the maximum $\dot{M}^{max}$. They have adapted the $\dot{M}(P_{orb})$ functional relationship of Mestel & Spruit (1987) to give

$$\dot{M}^{max} = 10^{18} \left(\frac{P_{orb}}{4\ \mathrm{h}}\right)^{5/2} \mathrm{g\ s^{-1}} \quad \text{for} \quad 3 < P_{orb} < 10\ \mathrm{h}. \qquad (12)$$

For AE Aqr, $P_{orb} = 9.88$ h, so that $\dot{M}^{max} = 10^{19}$ g s^{-1} is expected, giving $\mu \sim 5 \times 10^{32}$ $(\dot{M}^{eq}/\dot{M}^{max})^{1/2}$ G cm^3 when using equation (11). It is interesting to see that this relationship explains why the three DQ Her type objects lie on a straight line on the P_{spin} versus P_{orb} graph, requiring $\mu \sim 2 \times 10^{32}$ G cm^3.

The fact that AE Aqr is one of the DQ Her and intermediate polars with the smallest $\dot{M}$ at present is then also consistent with what we have inferred: $\dot{M}^{present} \ll \dot{M}^{eq} < \dot{M}^{max}$. Thus the present state of rapid spindown can, in principle, be explained in terms of $\dot{M}$ cycling in CVs, with AE Aqr currently being in a low state. A similar situation was proposed for Sco X-1 by Priedhorsky (1986), where pulsar-like spindown is the main source of energy during quiescence.

De Jager (1994) discussed a braking mechanism which may be responsible for the rapid spindown. In a pulsar, the spindown power is lost through a mixture of magnetic dipole radiation and the ejection of particles, and in a few cases via γ-radiation. In the case of AE Aqr, de Jager (1994) has shown that the 'dead disc' (or slowly accreting) model of Michel & Dressler (1981) may be applicable to AE Aqr, where a return current to the compact object is facilitated by the conducting disc. The short spin period, the value of μ inferred above and the lack of angular momentum transferred to the white dwarf by the disc (which lies outside the corotation radius) would then be sufficient to drive a wind with relativistic particles, which in turn removes kinetic energy from the white dwarf. The movement of relativistic electrons across the magnetic field may also explain the observations of steady and flare-like radio synchrotron emission. De Jager (1994) also remarked that the low $\dot{M}$ in AE Aqr results in a tenuous magnetosphere, and the formation of a double layer (a large electric field) would be possible provided that the current density in the tenuous magnetosphere was large enough. The potential drop may easily exceed a tera-electronvolt, which would explain the reports of quasi-periodic and burst-like TeV γ-rays from this system.

ACKNOWLEDGMENTS

We express our warmest words of thanks to E. Nather, F. Jablonski, B. Warner, M. Cropper, D. A. Buckley and C. Koen for providing us with published and unpublished data, M. Eracleous and K. Horne for providing us with valuable (unpublished) pulse timings, C. Brink for helping us with the Heliocentric corrections, J. F. Chandler for providing us with the PEP740 software for barycentric corrections, and J. N. Imamura, B. Warner and W. F. Welsh for valuable discussions.

REFERENCES

Abada-Simon M., Lecacheux A., Bastian T. S., Bookbinder J. A., Dulk G. A., 1993, ApJ, 406, 692
Bailey J., 1981, MNRAS, 197, 31
Bastian T. S., Dulk G. A., Chanmugam G., 1988, ApJ, 324, 431
Bookbinder J. A., Lamb D. Q., 1987, ApJ, 323, L131
Bowden C. C. G. et al., 1992, Astropart. Phys., 1, 47
de Jager O. C., 1991, ApJ, 378, 286
de Jager O. C., 1994, ApJS, 90, 775
Downs G. S., 1981, ApJ, 249, 687
Eracleous M., Patterson J., Halpern J., 1991, ApJ, 370, 330
Feldt A. N., Chincarini G., 1980, PASP, 92, 528
Ghosh P., Lamb F. K., 1979, ApJ, 234, 296
Ghosh P., Lamb F. K., 1991, in Ventura J., Pines D., ed., Neutron Stars: Theory and Observation, NATO ASI Series, Vol. 344. Kluwer, Dordrecht, p. 363
Imamura J. N., Steiman-Cameron T. Y., 1988, AJ, 96, 1420
Jablonski F., 1981, Inf. Bull. Variable Stars, 1911
Marsh T. R., 1992, MNRAS, 259, 695
Meintjes P. J., Raubenheimer B. C., de Jager O. C., Brink C., Nel H. I., North A. R., van Urk G., Visser B., 1992, ApJ, 401, 325
Mestel L., Spruit H. C., 1987, MNRAS, 226, 57
Michel F. C., Dessler A. J., 1981, ApJ, 251, 564
Nather R. E., 1973, Vistas Astron., 15, 91
Patterson J., 1979, ApJ, 324, 978 (P79)
Patterson J., Branch D., Chincarini G., Robinson E. L., 1980, ApJ, 240, L133
Patterson J., Beuerman K., Africano J., 1988, BAAS, 20, 1099
Payne-Gaposchkin C., 1969, ApJ, 158, 429
Priedhorsky W., 1986, ApJ, 306, L79
Robinson E. L., Shafter A. W., Balachandran S., 1991, ApJ, 374, 298 (RSB)
Warner B., 1987, MNRAS, 227, 23
Warner B., Wickramasinghe D. T., 1991, MNRAS, 248, 370
Webbink R. F., 1990, in Mauche C. W., ed., Accretion-powered Compact Binaries. Cambridge Univ. Press, Cambridge, p. 177
Welsh W. F., Horne K., Oke J. B., 1993, ApJ, 406, 229
Welsh W. F., Horne K., Gomer R., 1993, ApJ, 410, L39 (WHG)